

Results from an Einstein@Home search for continuous gravitational waves from G347.3 at low frequencies in LIGO O2 data

J. MING,^{1,2} M.A. PAPA,^{1,3,2} H.-B. EGGENSTEIN,^{1,2} B. MACHENSCHALK,^{1,2} B. STELTNER,^{1,2} R. PRIX,^{1,2} B. ALLEN,^{1,3,2} AND O. BEHNKE^{1,2}

¹*Max Planck Institute for Gravitational Physics (Albert Einstein Institute), Callinstrasse 38, D-30167 Hannover, Germany*

²*Leibniz Universität Hannover, D-30167 Hannover, Germany*

³*University of Wisconsin Milwaukee, 3135 N Maryland Ave, Milwaukee, WI 53211, USA*

ABSTRACT

We present results of a search for periodic gravitational wave signals with frequency between 20 and 400 Hz, from the neutron star in the supernova remnant G347.3-0.5, using LIGO O2 public data. The search is deployed on the volunteer computing project Einstein@Home, with thousands of participants donating compute cycles to make this endeavour possible. We find no significant signal candidate and set the most constraining upper limits to date on the amplitude of gravitational wave signals from the target, corresponding to deformations below 10^{-6} in a large part of the band. At the frequency of best strain sensitivity, near 166 Hz, we set 90% confidence upper limits on the gravitational wave intrinsic amplitude of $h_0^{90\%} \approx 7.0 \times 10^{-26}$. Over most of the frequency range our upper limits are a factor of 20 smaller than the indirect age-based upper limit.

Keywords: gravitational waves — continuous — SNRs — G347.3-0.5 — neutron stars

1. INTRODUCTION

Continuous gravitational waves are among the gravitational wave signals that have not yet been detected. Fast spinning neutron stars with non-axisymmetric deformations or with unstable r-modes are expected to emit continuous waves which lie in the high-sensitivity frequency range of ground-based interferometers (Owen et al. 1998; Owen 2010; Lasky 2015).

Although the expected waveforms are fairly simple, the search for continuous wave signals is very challenging due to their extreme weakness. Signal-to-noise ratio (SNR) is accumulated by integrating the signal over many months, and this increases our ability to resolve different waveforms. This also means that if the signal waveform is not a priori known, many different waveforms must be searched for, and the computing cost increases very significantly. In fact, when searching a broad range of waveforms, the sensitivity of continuous wave searches is usually limited by the computing power.

Since the Advanced LIGO (Abbott et al. 2015) detectors begun observations, various continuous waves searches have been carried out. Among them, the searches for continuous waves from known pulsars, with known spin frequency and frequency evolution, are the most sensitive and computationally inexpensive (Abbott et al. 2019a, 2021a; Ashok et al. 2021). At the other extreme, there are the all-sky surveys with no prior information of frequency and sky location (Dergachev & Papa 2021a, 2020, 2021b; Steltner et al. 2021b; Abbott et al. 2019b, 2021b,c; Covas & Sintès 2020). In-between, the directed searches target locations in the sky that are known or suspected to harbour a neutron star, albeit pulsation have generally not been observed. Searches of this type include the galactic centre (Piccinni et al. 2020; Dergachev et al. 2019), young supernova remnants (SNRs) (Ming et al. 2019; Papa et al. 2020; Abbott et al. 2019c; Millhouse et al. 2020; Lindblom & Owen 2020; Abbott et al. 2021d), glitching pulsars (Fesik & Papa 2020; Abbott et al. 2021e) and low-mass X-ray binaries such as Scorpius X-1 (Zhang et al. 2021).

Young neutron stars are good continuous wave candidates : an indirect upper limit can be placed on continuous gravitational wave strength that is proportional to $1/\sqrt{\tau}$, with τ being the age of the neutron star (Wette

jing.ming@aei.mpg.de

maria.alessandra.papa@aei.mpg.de

et al. 2008; Zhu et al. 2016). Fifteen young supernova remnants have been identified in our Galaxy that could host a young neutron star and potentially be promising targets. Recent searches probe emission from *all* of these over a broad range of waveforms (Lindblom & Owen 2020; Abbott et al. 2021d).

An alternative approach is to identify the most promising targets and concentrate the search efforts on these. In Ming et al. (2016) we propose an optimisation scheme to decide how to spend the computing budget in such a way to maximise the detection probability. With a computing budget of a few months on the Einstein@Home volunteer computing project, the indication is to search for emission from the neutron star in the SNRs Vela Jr. (G266.2-1.2), Cassiopeia A (G111.7-2.1) and G347.3 (G347.3-0.5). We carried out searches using O1 data, and O2 data for follow-ups, and set the most constraining upper limits on gravitational wave emission from these sources with those data (Ming et al. 2019; Papa et al. 2020).

In Papa et al. (2020), we also found a sub-threshold candidate at around 369 Hz. Gravitational wave follow-ups were not completely conclusive and we found no evidence of pulsations from searches of archival X-ray data to validate this candidate, but the X-ray searches had limited sensitivity. Abbott et al. (2021d) did not find this candidate in the first half of O3 data, however the sensitivity of Abbott et al. (2021d) is lower than that of our original search. We thus prioritize a deep search for G347.3 in the O2 data below 400 Hz. This paper presents results from such a search.

The paper is organised as follows: in Section 2 we review the astrophysical target and the model gravitational waveform. After a brief description of the data in Section Section 3, in Section 4 we describe the search. The results follow in Section 5, where we explain how the $h_0^{90\%}$ intrinsic continuous gravitational wave amplitude upper limits are derived. These are also recast as upper limits on the star’s ellipticity and r-mode saturation. We conclude with a discussion of the results, comparing and contrasting with existing literature in Section 6.

2. THE TARGET

2.1. G347.3-0.5

The supernova remnant G347.3 is suggested to be the remnant of the AD393 “guest star” (Wang et al. 1997). We therefore assume an age of 1600 years, albeit this estimate is not completely uncontroversial (Fesen et al. 2012). Using XMM data, Cassam-Chenaï et al. (2004) estimate its distance to be around 1.3 kpc. The position of the central compact object in the G347.3 SNR is given with sub-arcsecond accuracy in Mignani et al.

(2008), based on Chandra data. Among the SNRs in our galaxy, G347.3 is one of the most interesting directed search targets because of its relatively young age and close distance (Ming et al. 2016).

In the deep CW search for G347.3 in O1 data (Papa et al. 2020), we find an interesting candidate at around 369 Hz. The spin-down energy loss from the candidate parameters yields an unusually high value, 1.6×10^{40} erg/s, which exceeds the most energetic Crab pulsar’s $\dot{E} = 4.6 \times 10^{38}$ erg/s and J0537-6910’s $\dot{E} = 4.9 \times 10^{38}$ erg/s.

2.2. The Signal

We assume a standard IT2 continuous gravitational wave signal (Dergachev & Papa 2021b) produced by asymmetric rotating neutron stars which, in the detector data, has a form (Jaranowski et al. 1998):

$$h(t) = F_+(t)h_+(t) + F_\times(t)h_\times(t), \quad (1)$$

where $F_+(t)$ and $F_\times(t)$ are the antenna pattern functions of the detector for the two gravitational wave polarizations “+” and “ \times ”. They depend on the sky position of the source (defined by the right ascension α and declination δ), and the orientation ψ of the wave-frame with respect to the detector frame. $F_+(t)$ and $F_\times(t)$ are periodic time functions with a period of one sidereal day, because the detector rotates with the Earth.

The phase $\Phi(t)$ of the signal at solar system barycenter (SSB) frame has the form:

$$\Phi(\tau_{\text{SSB}}) = \Phi_0 + 2\pi[f(\tau_{\text{SSB}} - \tau_{0\text{SSB}}) + \frac{1}{2}\dot{f}(\tau_{\text{SSB}} - \tau_{0\text{SSB}})^2 + \frac{1}{6}\ddot{f}(\tau_{\text{SSB}} - \tau_{0\text{SSB}})^3], \quad (2)$$

where f is the signal frequency and τ_{SSB} is the arrival time of the GW front at the SSB frame.

3. THE DATA

The LIGO O2 public data (LIGO 2019; Abbott et al. 2021f) is used in this search. The data is from the two observatories in the USA, one in Hanford (Washington State) and the other in Livingston (Louisiana). The data used in this search is between GPS time 1167983370 (Jan 09 2017) and 1187731774 (Aug 25 2017). Short Fourier transforms (SFTs) of data segments 1800 seconds long (Allen & Mendell 2004) are created as customary for Einstein@Home searches.

Calibration lines, the mains power lines and some other spurious noise due to the LIGO laser beam jitter are removed in the publicly released O2 data (Davis et al. 2019). Additionally we remove loud short-duration glitches with the gating procedure described in Steltner

et al. (2021a) and substitute Gaussian noise in the frequency domain in disturbed bins. This is a standard procedure in Einstein@Home searches.

4. THE SEARCH

We use a “stack-slide” type of search based on the GCT (Global correlation transform) method (Pletsch & Allen 2009; Pletsch 2008, 2010). The data is partitioned in N_{seg} segments and each segment spans a duration T_{coh} . The data of both detectors from each segment i is searched with a maximum likelihood coherent method to construct the detection statistic, \mathcal{F} -statistic (Cutler & Schutz 2005). The statistics \mathcal{F}_i from the coherent searches of the different segments are summed, and the value of the core detection statistic $\bar{\mathcal{F}}$ is obtained:

$$\bar{\mathcal{F}} := \frac{1}{N_{\text{seg}}} \sum_{i=1}^{N_{\text{seg}}} \mathcal{F}_i. \quad (3)$$

In Gaussian noise $N_{\text{seg}} \times 2\bar{\mathcal{F}}$ follows a chi-squared distribution with $4N_{\text{seg}}$ degrees of freedom, and a non-centrality parameter ρ^2 . If a signal is present, ρ^2 is proportional to $\frac{h_0^2 T_{\text{obs}}}{S_h}$, where S_h is the strain power spectral density of the noise at the frequency of the signal, and h_0 is the signal intrinsic amplitude at Earth (Jaranowski et al. 1998).

The data in reality is not Gaussian and despite the removal of loud glitches and lines, some coherent disturbances persist. The $\bar{\mathcal{F}}$ can be effected by these coherent disturbances and present increased values. In order to identify occurrences of this, a line robust detection statistic $\hat{\beta}_{\text{S/GLtL}}$ (Keitel et al. 2014; Keitel 2016) is computed. This statistic is the log of a Bayesian odds ratio that tests the signal hypothesis versus an extended noise hypothesis. The noise model of this statistic not only includes Gaussian noise, but also coherent single-detector signals. The Einstein@Home results from this search are ranked according to $\hat{\beta}_{\text{S/GLtL}}$, such that the top-list contains fewer candidates which are affected by the coherent disturbances.

The search set-up, i.e. the coherent baseline T_{coh} , the template grid spacings and the search ranges are all derived from the optimisation procedure.

We search for signal-waveforms with frequency and frequency-derivatives as follows:

$$\begin{cases} 20 \text{ Hz} \leq f \leq 400 \text{ Hz} \\ -f/\tau \leq \dot{f} \leq 0 \text{ Hz/s} \\ 0 \text{ Hz/s}^2 \leq \ddot{f} \leq 7|\dot{f}|_{\text{max}}^2/f = 7f/\tau^2, \end{cases} \quad (4)$$

where $\tau = 1600$ years. The ranges for \dot{f} and \ddot{f} correspond to different breaking index n values, namely 2

and 7. In the \dot{f} equation the $n = 2$ is used to encompass the broadest range of \dot{f} values. In the \ddot{f} equation $n = 7$ is used to encompass all astrophysical scenarios including the phase evolution purely due to GW emission ($n = 5$) and r-mode oscillations ($n = 7$). At 400 Hz, the \dot{f} extends down to -8.0×10^{-9} Hz/s and the \ddot{f} range up to 1.1×10^{-18} Hz/s².

The grid spacings in frequency and spin-downs are constant over these search ranges and are given in Table 1. The number of searched templates per 1 Hz band increases as the frequency increases, as Eq. 4 shows. Fig. 1 shows the number of templates searched in 1-Hz bands as a function of frequency.

The search is performed on the Einstein@Home volunteer computing project. Einstein@Home is built on the BOINC (Berkeley Open Infrastructure for Network Computing) architecture (Anderson 2004; Anderson et al. 2006) which uses the idle time on volunteer computers to tackle scientific problems such as this, that require large amounts of computing power.

Overall we search $\approx 5.1 \times 10^{16}$ templates, utilizing Einstein@Home for several weeks. The work-load is split in work-units, sized to keep the average volunteer host busy for 8 hours. The whole search task is split into about 2.5 million work-units. Only information from the most promising 10000 results from each work-unit is communicated back to the central Einstein@Home server.

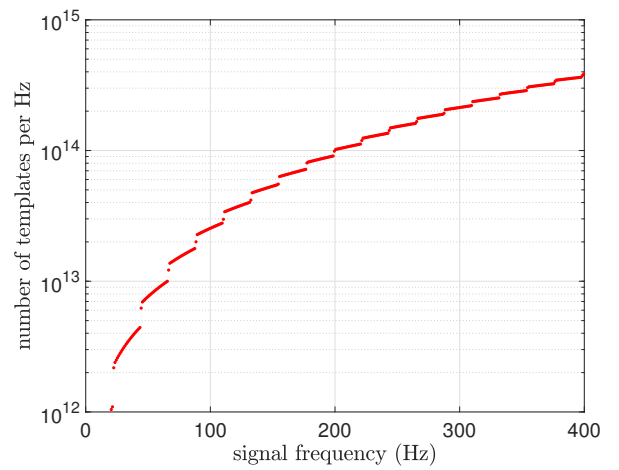


Figure 1. Number of templates searched in 1-Hz bands as a function of signal frequency.

5. RESULTS

After the Einstein@Home server has received all search results, the post-processing begins. In total we have 2.5 million work-units \times 10 000 results returned per work-unit $\approx 2.5 \times 10^{10}$

SEARCH SET-UP					
$T_{\text{coh}} = 1080$ hr	$N_{\text{seg}} = 5$	$\delta f = 1.3 \times 10^{-7}$ Hz	$\delta \dot{f} = 1.5 \times 10^{-14}$ Hz/s	$\delta \ddot{f} = 1.2 \times 10^{-20}$ Hz/s ²	$T_{\text{ref}} = 1177858472.0^{\text{a}}$

^a Barycentric Dynamical Time in GPS seconds

Table 1. Spacings on the signal parameters used for the templates in the search.

search results. Each result is identified by the template-waveform parameters (f, \dot{f}, \ddot{f}) and by the detection statistics values.

With a parameter-space clustering procedure we identify the most interesting results (Steltner et al. 2021b; A. Singh & Walsh 2017; Beheshtipour & Papa 2020, 2021). We refer to these as ‘‘candidates’’. We consider the top 1 million candidates, corresponding to a detection statistic threshold $\hat{\beta}_{\text{S/GLtLr}} = 1.948$.

The distribution of the detection statistic $\hat{\beta}_{\text{S/GLtLr}}$ and $2\mathcal{F}_r$ for these candidates is shown in Figure 2. We use $\hat{\beta}_{\text{S/GLtLr}}$ to rank our candidates but also show $2\mathcal{F}_r$ because its distribution in Gaussian noise is known. A detectable signal would look like an obvious outlier in both distributions. In Figures 2 we instead see an outlier in the $2\mathcal{F}_r$ distribution but not in the $\hat{\beta}_{\text{S/GLtLr}}$ distribution. This is an indication that a coherence in one of the two detectors is causing the high value of $2\mathcal{F}_r$. In particular the $2\mathcal{F}_r$ outlier has a value of 32.9, whereas its $\hat{\beta}_{\text{S/GLtLr}} = 2.0$ which is in 5th percentile of lowest values. We follow-up this candidate with a semi-coherent search with $T_{\text{coh}} = 2760$ hr. The most significant result $2\mathcal{F}_r = 54.6$ falls short of what one would expect from a signal: none of the over thousand signals tested showed this small increase in signal-to-noise ratio. After excluding this candidate, Figures 2 shows no significant signal candidate in either $2\mathcal{F}_r$ or $\hat{\beta}_{\text{S/GLtLr}}$.

5.1. Upper limits

We determine the smallest h_0 that would have produced a detection statistic as high as the most significant measured in every half Hz band. We assume the source to be at the position of our target, the spindown to be in the target range and the frequency varying in each half Hz. We set the confidence level at 90%, meaning that 90% of the signals in the considered range with an amplitude at the upper limit value $h_0^{90\%}$, would yield a value of the detection statistic larger than the loudest search result from that parameter range. We use the $\hat{\beta}_{\text{S/GLtLr}}$ as our reference statistic, since it is our ranking statistic.

In each half Hz band, 200 simulated signals with a fixed value of the intrinsic amplitude h_0 are added to the real detector data. The data is then processed as the data that was searched, i.e. it is gated and line-cleaned.

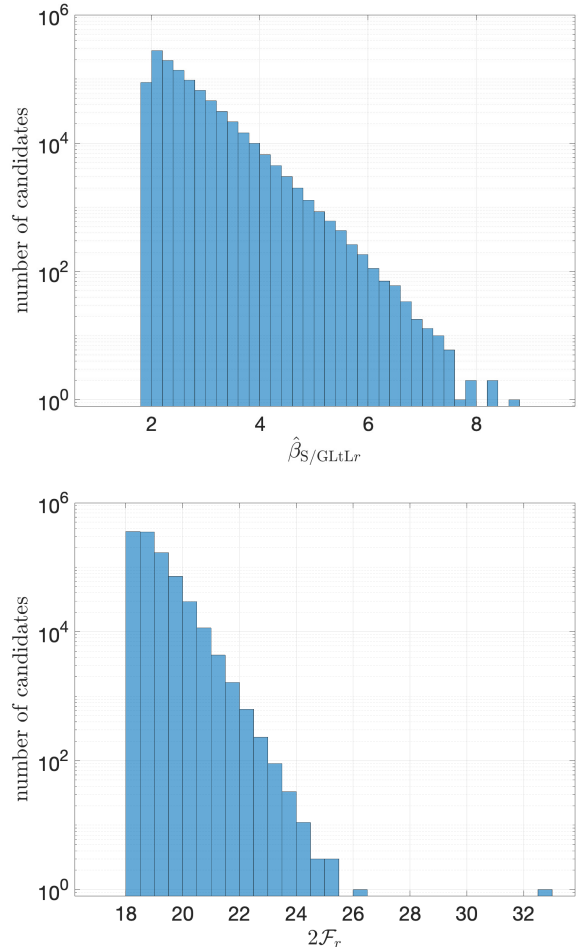


Figure 2. Distribution of the detection statistics $\hat{\beta}_{\text{S/GLtLr}}$ (top) and $2\mathcal{F}_r$ (bottom) of the top 1 million candidates ranked according to $\hat{\beta}_{\text{S/GLtLr}}$, which is the line- and transient-line-robust statistic.

The parameters of simulated signals, the frequency, inclination angle $\cos \iota$, polarization ψ and initial phase values, are uniformly randomly distributed in their respective ranges. The spin-down values, \dot{f} and \ddot{f} , are log-uniformly randomly distributed in their respective ranges.

A search is performed to recover each injection with the same grid and set-up as the original Einstein@Home search. The search is more limited than the original search to save computations, and covers the parameter space neighbouring the fake signal. The fake signal is counted as recovered if the $\hat{\beta}_{\text{S/GLtLr}}$ from the search

is higher than the maximum $\hat{\beta}_{S/GLtLr}$ from the Einstein@Home results in the same half Hz band.

This whole procedure is repeated for various values of h_0 . For each value of h_0 , the fraction of detected injections is determined in this way and varying h_0 the confidence $C(h_0)$ curve is constructed. We use a fit with a sigmoid of the form:

$$C(h_0) = \frac{1}{1 + \exp\left(\frac{a-h_0}{b}\right)}, \quad (5)$$

and from it we read-off the h_0 amplitude that corresponds to 90% confidence, our upper limit value.

The Matlab nonlinear regression prediction confidence intervals routine `nlpredci` is used to yield the best-fit for a and b values and the covariance matrix. This covariance matrix can be used to compute the 95% credible interval on the fit of $h_0^{90\%}$. Figure 3 shows the sigmoid curve fitting for the 149-149.5 Hz band, as a representative example of the results obtained with this procedure. The best fit for $h_0^{90\%}$ in this band is 7.5×10^{-26} . The uncertainties introduced by this procedure are less than 4%. The total uncertainty in the upper limit is the sum of the fitting procedure uncertainty and the calibration uncertainties. We conservatively use 5% as the calibration uncertainty (Cahillane et al. 2017).

The $h_0^{90\%}$ upper limits are shown in Figure 4 and provided in machine readable format at Ming et al. (2021).

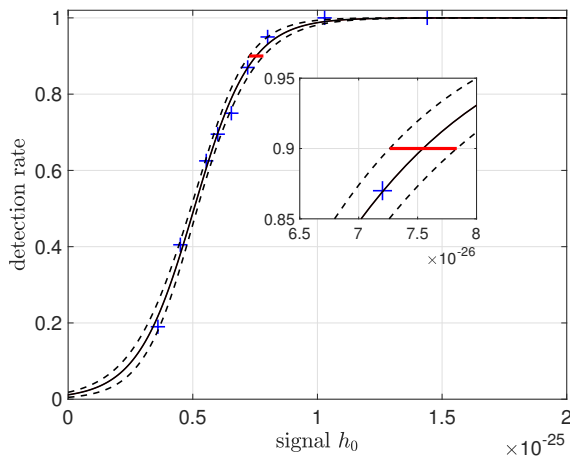


Figure 3. Blue crosses: measured detection efficiency $C(h_0)$ from search-and-recovery Monte Carlos in the frequency band 149 to 149.5 Hz. The solid line is the best fit and the dashed lines represent 95% confidence intervals on the fit. The red line marks the 90% detection rate, with the uncertainties introduced by this fitting procedure 4%. The inset shows a zoom around the 90% confidence level.

In nineteen half-Hz bands we do not set an upper limit; correspondingly in the upper limit files we have 741 en-

tries rather than 760. The cleaning procedure substitutes disturbed frequency-domain data with Gaussian noise in order to avoid further spectral contamination from “leakage” in the search results. Those bands are consistently cleaned in the upper-limit Monte Carlos after a signal is injected, so it may happen that most of the injected signal is removed. When that happens, no matter how loud the signal is, the detection efficiency does not increase. In these bands the 90% detection rate level cannot be reached and we do not set any upper limit. This reflects the fact that, even if we had a signal there, because of the cleaning procedure, we could not detect it.

In other bands the cleaning procedure partly or completely removes some of the signals, depending on their frequency. So, in order to produce a detection statistic value above a given threshold, statistically, a louder signal is required than in nearby bands that are not cleaned. In those bands the upper limit is higher than what it would be if the data had not been cleaned. For example, $h_0^{90\%}$ of the band 331 - 331.5 Hz is about 15% larger than the $h_0^{90\%}$ of the neighbor half Hz bands. In this bands 8% of the data is Gaussian noise data.

5.2. Upper limits on the astrophysical parameters

The h_0 upper limits can be converted in constraints on the equatorial ellipticity ε of the neutron star at a distance D and at frequency f (Zimmermann & Szedenits 1979):

$$\varepsilon = \frac{c^4}{4\pi^2 G} \frac{h_0 D}{I f^2}, \quad (6)$$

where c is the speed of light, G is the gravitational constant and I the principal moment of inertia of the star. Assuming a fiducial value of the principal moment of inertia of 10^{38} kg m^2 and $D = 1.3 \text{ kpc}$, we convert $h_0^{90\%}(f)$ into upper limits on the ellipticity of the source G347.3. These are shown in Figure 5.

R-mode oscillations of a spinning neutron stars also produce continuous gravitational waves. The amplitude h_0 for a signal with frequency f , from a source at a distance D , depend on the r-mode amplitude α as follows (Owen 2010):

$$\alpha = 0.028 \left(\frac{h_0}{10^{-24}} \right) \left(\frac{D}{1 \text{ kpc}} \right) \left(\frac{100 \text{ Hz}}{f} \right)^3. \quad (7)$$

Our $h_0^{90\%}$ upper limits can then be recast as upper limits on the r-mode amplitude. The result is shown in Figure 6.

6. CONCLUSIONS

In this paper we present results from the most sensitive search to date for continuous gravitational wave

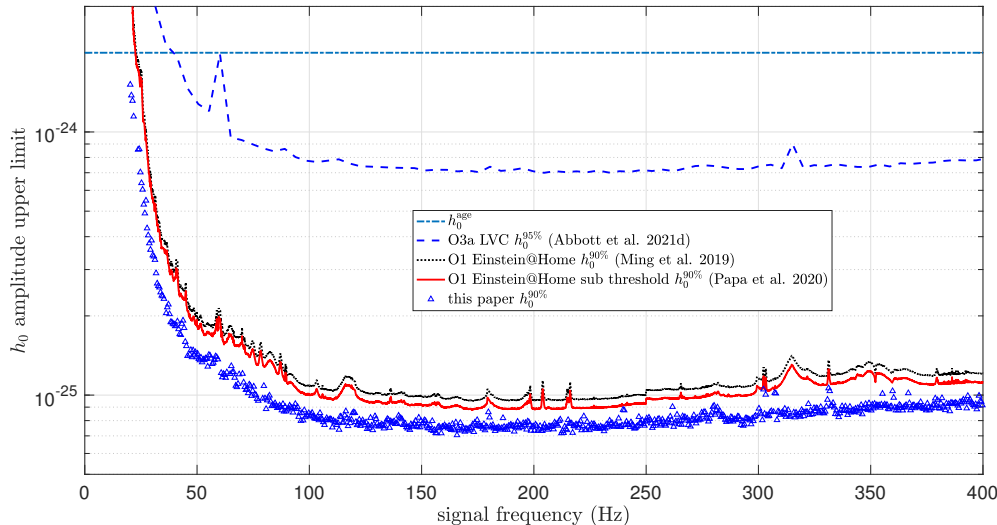


Figure 4. 90% confidence upper limits on the gravitational wave amplitude of continuous gravitational wave signals from G347.3 for signals with frequency between 20 to 400 Hz. The lower blue triangles are the results of this search and we compare them with results from previous searches: The blue dots are the upper limits from the LVC search of the O3a (Abbott et al. 2021d); The black dots are Einstein@Home results from O1 data (Ming et al. 2019) and red solid line the sub-threshold search (Papa et al. 2020).

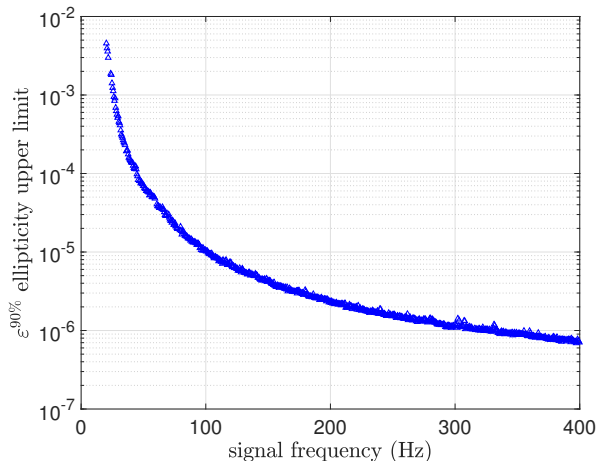


Figure 5. Upper limits on the equatorial ellipticity of G347.3. We assume a distance of 1.3 kpc.

emission from the supernova remnant G347.3-0.5 in the frequency range 20-400 Hz and the broadest first and second frequency-derivative range. Electro-magnetic pulsations have not been detected from this object, and the direct observation of continuous gravitational emission would provide the first gravitational wave pulsar timing solution.

We prioritize this target with respect to other SNRs because of a sub-threshold candidate from a previous search. We do not find a signal.

We constrain the amplitude of continuous gravitational wave emission at a level which is more than a

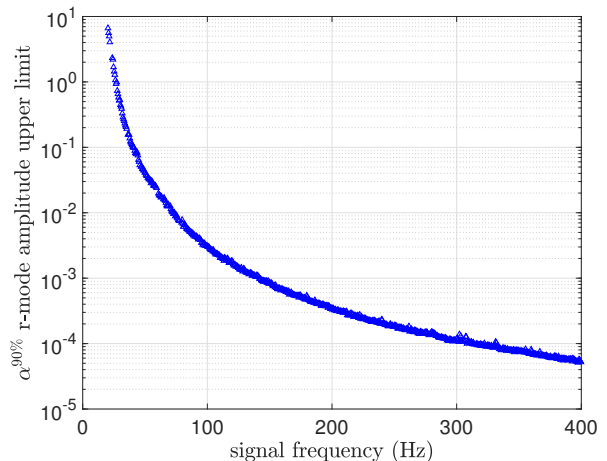


Figure 6. Upper limits on the r-mode amplitude.

factor of 20 smaller than the indirect age-based limit over most of the frequency range. The most constraining intrinsic gravitational wave amplitude upper limit is 7.0×10^{-26} near 166 Hz. This result improves over our O1 result (Ming et al. 2019) and over the extensive sub-threshold O1 search (Papa et al. 2020). It is also more constraining than the recent search result of Abbott et al. (2021d) that uses the significantly more sensitive O3a data. In fairness we note however Abbott et al. (2021d) search a broader frequency range and their search uses a technique that is more robust to possible deviations of the signal from the IT- n model.

Recast in terms of equatorial ellipticity of the neutron star, our results constrain it below 10^{-6} at frequencies higher than ≈ 320 Hz reaching bounds of 6.9×10^{-7} at 400 Hz. This is a physically plausible value of neutron star deformation (Johnson-McDaniel & Owen 2013; Gittins et al. 2020; Gittins & Andersson 2021). Such limit is not matched in Abbott et al. (2021d) even at 2000 Hz.

Our spindown range is high enough to allow for braking indexes as high as 7, encompassing r-mode emission. Our null result can then constrain the r-mode amplitude and does so at a level below 10^{-4} at frequencies higher than ≈ 310 Hz. This is also a physically possible value (Haskell 2015).

This is the first O2 public-data Einstein@Home search for continuous gravitational waves from SNRs and probes a physically interesting range of source parameters. Building on this, future searches will extend the parameters space and/or include more targets and/or more data, pushing further in interesting territory.

7. ACKNOWLEDGMENTS

We gratefully acknowledge the support of the many thousands of Einstein@Home volunteers who made this search possible.

We acknowledge support from the Max Planck Society for Projects QPQ10003 and QPQ10004, and the NSF grant 1816904.

A lot of post-processing is run on the ATLAS cluster at AEI Hannover. We thank Carsten Aulbert and Henning Fehrmann for their support.

We would like to thank the instrument-scientist and engineers of LIGO whose amazing work has produced detectors capable of probing gravitational waves so incredibly small.

This research has made use of data, software and/or web tools obtained from the Gravitational Wave Open Science Center (<https://www.gw-openscience.org/>), a service of LIGO Laboratory, the LIGO Scientific Collaboration and the Virgo Collaboration. LIGO Laboratory and Advanced LIGO are funded by the United States National Science Foundation (NSF) as well as the Science and Technology Facilities Council (STFC) of the United Kingdom, the Max-Planck-Society (MPS), and the State of Niedersachsen/Germany for support of the construction of Advanced LIGO and construction and operation of the GEO600 detector. Additional support for Advanced LIGO was provided by the Australian Research Council. Virgo is funded, through the European Gravitational Observatory (EGO), by the French Centre National de Recherche Scientifique (CNRS), the Italian Istituto Nazionale di Fisica Nucleare (INFN) and the

Dutch Nikhef, with contributions by institutions from Belgium, Germany, Greece, Hungary, Ireland, Japan, Monaco, Poland, Portugal, Spain.

REFERENCES

- A. Singh, M. A. Papa, H. B. E., & Walsh, S. 2017, *Phys. Rev. D*, 96, 082003, doi: [10.1103/PhysRevD.96.082003](https://doi.org/10.1103/PhysRevD.96.082003)
- Abbott, B. P., et al. 2015, *Classical and Quantum Gravity*, 32, 074001, doi: [10.1088/0264-9381/32/7/074001](https://doi.org/10.1088/0264-9381/32/7/074001)
- . 2019a, *The Astrophysical Journal*, 879, 10, doi: [10.3847/1538-4357/ab20cb](https://doi.org/10.3847/1538-4357/ab20cb)
- . 2019b, *Phys. Rev. D*, 100, 024004, doi: [10.1103/PhysRevD.100.024004](https://doi.org/10.1103/PhysRevD.100.024004)
- . 2019c, *The Astrophysical Journal*, 875, 122, doi: [10.3847/1538-4357/ab113b](https://doi.org/10.3847/1538-4357/ab113b)
- . 2021a, *The Astrophysical Journal Letters*, 913, L27, doi: [10.3847/2041-8213/abffcd](https://doi.org/10.3847/2041-8213/abffcd)
- . 2021b, *Phys. Rev. D*, 103, 064017, doi: [10.1103/PhysRevD.103.064017](https://doi.org/10.1103/PhysRevD.103.064017)
- Abbott, R., et al. 2021c. <https://arxiv.org/abs/2107.00600>
- . 2021d. <https://arxiv.org/abs/2105.11641>
- . 2021e. <https://arxiv.org/abs/2104.14417>
- . 2021f, *SoftwareX*, 13, 012021, doi: <https://doi.org/10.1016/j.softx.2021.100658>
- Allen, B., & Mendell, G. 2004, SFT Data Format Version 2 Specification, <https://dcc.ligo.org/LIGO-T040164/public>
- Anderson, D. P. 2004, in *Proceedings of the Fifth IEEE/ACM International Workshop on Grid Computing (GRID04)*, 4–10
- Anderson, D. P., Christensen, C., & Allen, B. 2006, in *Proceedings of the 2006 ACM/IEEE conference on Supercomputing*, 126–136
- Ashok, A., Beheshtipour, B., Papa, M. A., et al. 2021. <https://arxiv.org/abs/2107.09727>
- Beheshtipour, B., & Papa, M. A. 2020, *Phys. Rev. D*, 101, 064009, doi: [10.1103/PhysRevD.101.064009](https://doi.org/10.1103/PhysRevD.101.064009)
- . 2021, *Phys. Rev. D*, 103, 064027, doi: [10.1103/PhysRevD.103.064027](https://doi.org/10.1103/PhysRevD.103.064027)
- Cahillane, C., Betzwieser, J., Brown, D. A., et al. 2017, *Phys. Rev. D*, 96, 102001, doi: [10.1103/PhysRevD.96.102001](https://doi.org/10.1103/PhysRevD.96.102001)
- Cassam-Chenaï, G., Decourchelle, A., Ballet, J., et al. 2004, *A&A*, 427, 199, doi: [10.1051/0004-6361:20041154](https://doi.org/10.1051/0004-6361:20041154)
- Covas, P. B., & Sintes, A. M. 2020, *Phys. Rev. Lett.*, 124, 191102, doi: [10.1103/PhysRevLett.124.191102](https://doi.org/10.1103/PhysRevLett.124.191102)
- Cutler, C., & Schutz, B. F. 2005, *Phys. Rev.*, D72, 063006, doi: [10.1103/PhysRevD.72.063006](https://doi.org/10.1103/PhysRevD.72.063006)
- Davis, D., Massinger, T., Lundgren, A., et al. 2019, *Classical and Quantum Gravity*, 36, 055011, doi: [10.1088/1361-6382/ab01c5](https://doi.org/10.1088/1361-6382/ab01c5)
- Dergachev, V., & Papa, M. A. 2020, *Phys. Rev. Lett.*, 125, 171101, doi: [10.1103/PhysRevLett.125.171101](https://doi.org/10.1103/PhysRevLett.125.171101)
- . 2021a, *Phys. Rev. D*, 104, 043003, doi: [10.1103/PhysRevD.104.043003](https://doi.org/10.1103/PhysRevD.104.043003)
- . 2021b, *Phys. Rev. D*, 103, 063019, doi: [10.1103/PhysRevD.103.063019](https://doi.org/10.1103/PhysRevD.103.063019)
- Dergachev, V., Papa, M. A., Steltner, B., & Eggenstein, H.-B. 2019, *Phys. Rev. D*, D99, 084048
- Fesen, R. A., Kremer, R., Patnaude, D., & Milisavljevic, D. 2012, *AJ*, 143, 27, doi: [10.1088/0004-6256/143/2/27](https://doi.org/10.1088/0004-6256/143/2/27)
- Fesik, L., & Papa, M. A. 2020, *Astrophys. J.*, 895, 11, doi: [10.3847/1538-4357/ab8193](https://doi.org/10.3847/1538-4357/ab8193)
- Gittins, F., & Andersson, N. 2021. <https://arxiv.org/abs/2105.06493>
- Gittins, F., Andersson, N., & Jones, D. I. 2020, *Mon. Not. Roy. Astron. Soc.*, 500, 5570, doi: [10.1093/mnras/staa3635](https://doi.org/10.1093/mnras/staa3635)
- Haskell, B. 2015, *Int. J. Mod. Phys. E*, 24, 1541007, doi: [10.1142/S0218301315410074](https://doi.org/10.1142/S0218301315410074)
- Jaranowski, P., Krolak, A., & Schutz, B. F. 1998, *Phys. Rev.*, D58, 063001, doi: [10.1103/PhysRevD.58.063001](https://doi.org/10.1103/PhysRevD.58.063001)
- Johnson-McDaniel, N., & Owen, B. 2013, *Phys. Rev. D*, 88, 044004
- Keitel, D. 2016, *Phys. Rev.*, D93, 084024, doi: [10.1103/PhysRevD.93.084024](https://doi.org/10.1103/PhysRevD.93.084024)
- Keitel, D., Prix, R., Papa, M. A., Leaci, P., & Siddiqi, M. 2014, Search for continuous gravitational waves: Improving robustness versus instrumental artifacts, doi: [10.1103/PhysRevD.89.064023](https://doi.org/10.1103/PhysRevD.89.064023)
- Lasky, P. D. 2015, *Publications of the Astronomical Society of Australia*, 32, e034, doi: [10.1017/pasa.2015.35](https://doi.org/10.1017/pasa.2015.35)
- LIGO. 2019, The O2 Data Release, <https://www.gw-openscience.org/O2/>, doi: [10.7935/CA75-FM95](https://doi.org/10.7935/CA75-FM95)
- Lindblom, L., & Owen, B. J. 2020, *Phys. Rev. D*, 101, 083023, doi: [10.1103/PhysRevD.101.083023](https://doi.org/10.1103/PhysRevD.101.083023)
- Mignani, R. P., Zaggia, S., de Luca, A., et al. 2008, *A&A*, 484, 457, doi: [10.1051/0004-6361:20079076](https://doi.org/10.1051/0004-6361:20079076)
- Millhouse, M., Strang, L., & Melatos, A. 2020, *Phys. Rev. D*, 102, 083025, doi: [10.1103/PhysRevD.102.083025](https://doi.org/10.1103/PhysRevD.102.083025)
- Ming, J., Krishnan, B., Papa, M. A., Aulbert, C., & Fehrmann, H. 2016, *Phys. Rev.*, D93, 064011, doi: [10.1103/PhysRevD.93.064011](https://doi.org/10.1103/PhysRevD.93.064011)
- Ming, J., Papa, M. A., Singh, A., et al. 2019, *Phys. Rev.*, D100, 024063, doi: [10.1103/PhysRevD.100.024063](https://doi.org/10.1103/PhysRevD.100.024063)
- Ming, J., et al. 2021, www.aei.mpg.de/continuouswaves/O2G347-DirectedSearches
- Owen, B. J. 2010, How to adapt broad-band gravitational-wave searches for r-modes, doi: [10.1103/PhysRevD.82.104002](https://doi.org/10.1103/PhysRevD.82.104002)
- Owen, B. J., Lindblom, L., Cutler, C., et al. 1998, Gravitational waves from hot young rapidly rotating neutron stars, doi: [10.1103/PhysRevD.58.084020](https://doi.org/10.1103/PhysRevD.58.084020)

- Papa, M. A., Ming, J., Gotthelf, E. V., et al. 2020, *The Astrophysical Journal*, 897, 22, doi: [10.3847/1538-4357/ab92a6](https://doi.org/10.3847/1538-4357/ab92a6)
- Piccinni, O. J., Astone, P., D'Antonio, S., et al. 2020, *Phys. Rev. D*, 101, 082004, doi: [10.1103/PhysRevD.101.082004](https://doi.org/10.1103/PhysRevD.101.082004)
- Pletsch, H. J. 2008, *Phys. Rev. D*, 78, 102005. <https://arxiv.org/abs/0807.1324>
- . 2010, *Phys. Rev. D*, 82, 042002. <https://arxiv.org/abs/1005.0395>
- Pletsch, H. J., & Allen, B. 2009, *Phys. Rev. Lett.*, 103, 181102
- Steltner, B., Papa, M. A., & Eggenstein, H.-B. 2021a. <https://arxiv.org/abs/2105.09933>
- Steltner, B., Papa, M. A., Eggenstein, H.-B., et al. 2021b, *The Astrophysical Journal*, 909, 79, doi: [10.3847/1538-4357/abc7c9](https://doi.org/10.3847/1538-4357/abc7c9)
- Wang, Z. R., Qu, Q.-Y., & Chen, Y. 1997, *A&A*, 318, L59
- Wette, K., et al. 2008, *Class. Quant. Grav.*, 25, 235011, doi: [10.1088/0264-9381/25/23/235011](https://doi.org/10.1088/0264-9381/25/23/235011)
- Zhang, Y., Papa, M. A., Krishnan, B., & Watts, A. L. 2021, *The Astrophysical Journal*, 906, L14, doi: [10.3847/2041-8213/abd256](https://doi.org/10.3847/2041-8213/abd256)
- Zhu, S. J., et al. 2016, *Phys. Rev.*, D94, 082008, doi: [10.1103/PhysRevD.94.082008](https://doi.org/10.1103/PhysRevD.94.082008)
- Zimmermann, M., & Szedenits, E. 1979, *Phys. Rev. D*, 20, 351, doi: [10.1103/PhysRevD.20.351](https://doi.org/10.1103/PhysRevD.20.351)